Bioorganic & Medicinal Chemistry 16 (2008) 8224–8236

Contents lists available at ScienceDirect

Bioorganic & Medicinal Chemistry

journal homepage: www.elsevier.com/locate/bmc

Structure–activity relationships of new inhibitors of breast cancer resistance protein (ABCG2)

Anne Pick †, Henrik Müller †, Michael Wiese *

Institute of Pharmacy, University of Bonn, An der Immenburg 4, 53121 Bonn, Germany

ARTICLE INFO

Article history:
Received 28 April 2008
Revised 8 July 2008
Accepted 16 July 2008
Available online 20 July 2008

Keywords:
Breast cancer resistance protein
Multidrug resistance
Hoechst 33342 assay
3rd generation modulators
P-glycoprotein
XR9576 (tariquidar)
Quantitative structure–activity relationships
CoMFA
CoMSIA

ABSTRACT

At the end of the last century tariquidar (XR9576) was synthesized, pharmacologically investigated, and classified as a promising 3rd generation P-glycoprotein (P-gp) modulator. Following the discovery of BCRP in 1998 an increasing number of substances were studied in relation to their potency to interact with this transporter. Recently it has been shown that XR9576 inhibits both P-gp and BCRP transport function similarly to GF120918 (elacridar). This observation prompted us to investigate 5 XR compounds and 25 structurally related derivatives synthesized in our laboratory for their BCRP inhibitory effect. The biological activity data were determined by our new Hoechst 33342 assay that has been transferred from P-gp to BCRP overexpressing cells. 3D-QSAR models (CoMFA and CoMSIA) were generated and validated by the leave-many-out method and the scrambling stability test. The best models yielded an internal predictive squared correlation coefficient higher than 0.8 and contained steric, electrostatic, hydrophobic, and hydrogen bond donor fields. To our knowledge, this is the first 3D-QSAR analysis of BCRP inhibitors. Additionally the biological activity data determined in P-gp overexpressing cells on one side and BCRP overexpressing cells on the other side were compared to identify selective and non-selective inhibitors of P-gp and BCRP. The results may help to get a better insight which structural elements are necessary to direct the interaction of these compounds with P-gp and/or BCRP.

1. Introduction

Multidrug resistance is a major obstacle to successful cancer treatment by chemotherapy. One pivotal mechanism by which tumor cells can become resistant to cytotoxic drugs used in chemotherapy is the increased expression of certain ATP-binding cassette (ABC) transporters. These ABC transporters use the energy of ATP hydrolysis to transport a wide variety of substrates out of cells against a concentration gradient leading to a decreased intracellular concentration and in turn to failure of chemotherapy.

To date there have been 49 human ABC transporters identified and classified into seven subfamilies.[1] In humans, members from three subfamilies are primarily associated with the phenomenon of multidrug resistance (MDR). These include a member of the B- (ABCB1, P-glycoprotein), the G- (ABCG2, BCRP) and several members of the C-subfamily (ABCC1-5, MRPs).[2,3] As members of these three different subfamilies can be simultaneously overexpressed in tumor cells, MDR emerges frequently as a multifactorial, complex problem.

The MDR-related ABC transporters are widely expressed in excreting organs and physiological barriers such as the intestine, liver, kidney, blood–brain barrier and placenta, where they play a physiological key role in the protection against toxic agents.[4–6]

With regard to their physiological role, MDR-ABC transporters most probably evolved as complex cellular defense systems for the recognition and the energy-dependent removal of toxic agents entering the living cells or organisms from their environment. Therefore, they can be considered as essential parts of an immune-like defense system.[7] When expressed in tumor cells, ABC transporters such as P-gp, BCRP, and MRP1 cause multidrug resistance of such tumor cells. Therefore, it is in focus of research interest to overcome MDR-mediated resistance in cancer cells.

P-glycoprotein (P-gp) was discovered by Juliano and Ling in 1976[8] and is possibly the most intensely studied among the ABC transporters. In accordance with other ABC transporters, P-glycoprotein is a membrane-bound, energy-dependent drug transporter.[9] P-gp consists of 1280 amino acids and has a molecular weight of approximately 170 kDa in the fully glycosylated form.[10–12] The protein is folded into two homologous halves, each containing six transmembrane helices and one intracellular nucleotide binding domain (NBD). P-gp contains three glycosylation sites on an extracytoplasmatic domain[13], which have no essential role for transport function and serve to anchor the protein in the membrane.[10,11]

By actively effluxing substrates, P-gp reduces intracellular concentrations to subtherapeutic levels, thereby conferring resistance

* Corresponding author. Tel.: +49 228 735213; fax: +49 228 737929.
E-mail address: mwiese@uni-bonn.de (M. Wiese).
† These authors contributed equally.

0968-0896/$ - see front matter © 2008 Elsevier Ltd. All rights reserved.
doi:10.1016/j.bmc.2008.07.034

to a broad range of cytotoxic drugs. Its most striking property is the diversity in structure of substrates that can be transported, including a vast number of drugs, among them many cytotoxic anticancer drugs, such as anthracylines, *Vinca* alkaloids, taxanes, podophyllotoxin derivatives, and derivatives from *Campthoteca acuminata* (camptothecin, topotecan, irinotecan).[14,15] The consensus that has emerged is that P-gp-recognized substrates are amphipatic[7] with a molecular mass of 200–1900 Da.[10] In most cases anionic substrates show no interaction with P-gp.[10]

The breast cancer resistance protein (BCRP, ABCG2) was first identified as an overexpressed protein in the MCF-7/AdrVp cell line. This cell line was selected by continuous exposure to doxorubicin in combination with verapamil to avoid development of resistance due to expression of P-gp. Interestingly, MCF-7/AdrVp cells also did not express the multidrug resistance-associated protein MRP1.[16,17] BCRP was also discovered by investigating cell lines selected for resistance to mitoxantrone – a poor substrate for P-gp and MRP1.[18]

ABC transporters belonging to the subfamily G possess only one NBD and a single transmembrane domain (TMD), containing six membrane-spanning helices and thus are considered to be 'half transporters'. BCRP is composed of 655 amino acids and has a molecular weight of 72 kDa. It forms a homodimer probably linked by a disulfide bond in the membrane.[6] It migrates as a dimer without reducing agents on a SDS gel, but runs as a 72 kDa protein on a SDS gel under reducing conditions.[18,19] Further ABCG2 is extensively glycosylated on asparagine-596, which is located within the third extracellular loop of the polypeptide.[20–22] In accordance with P-gp, this glycosylation has no effect on transport function, but anchors the protein in the membrane. While the majority of ABC transporters include an N-terminal TMD followed by a C-terminal NBD, the ABCG2 protein has a reverse structure with the NBD located N-terminal to the TMD.[17] The structural differences serve to underline the importance of ABCG2 structural studies.

ABCG2 is not only expressed in cancer cells, but is also present in many normal tissues, for example, in the placenta, particularly in the syncytiotrophoblastic cells. The remarkable expression level of ABCG2 in the placenta led to the nomenclature ABCP, and suggests that ABCG2 is responsible for protecting the fetus from toxic xenobiotics.[23,24] Lower levels of BCRP were also found in the brain, in the colon, small intestine, breast tissue, testis, ovary, liver, and prostate. The tissue localization points to a physiologically protective role of BCRP.

In comparison to P-gp BCRP is able to efflux large molecules, both positively and negatively charged, with amphiphilic character. To the transported substrates belong sulfated hormone metabolites or glucuronidated methotrexate.[25–27] Further substrates of BCRP include the anticancer drugs mitoxanthrone, campthotecin-based topoisomerase 1 inhibitors such as topotecan or irinotecan, tyrosin kinase inhibitors such as imatinib and gefitinib, the podophyllotoxins etoposid and teniposid and flavopiridol.[28,6,29] A strategy to reverse BCRP-mediated multidrug resistance and to improve treatment outcome is the inhibition of this ABC protein with modulators showing high potency and efficacy. Selective inhibitors for BCRP include fumitremorgin C[6] and novobiocin.[30] More recently a non-toxic, synthetic analogue of fumitremorgin C, Ko143, has been identified as a potent and selective modulator of BCRP inhibiting BCRP at nanomolar concentrations.[31] Further, natural products are known to interact with BCRP. Investigations of Ahmed-Belkacem et al. illustrated that the flavonoids 6-prenylchrysin and tectochrysin can be considered as BCRP-specific inhibitors. For these compounds no interaction with P-gp or MRP1 was detected whereas low concentrations of these substances led to a distinct interaction with BCRP comparable to that of GF120918 (elacridar).[32] In another study, it was shown that the flavonoids narigenin and genistein possess higher inhibitory potencies towards BCRP than to MRP1 and P-gp.[33] These findings underline the importance of further investigations of flavonoids towards BCRP due to their potential specific interaction with this ABC-transporter. Though different in structure and genetic background, P-gp and BCRP share several common substrates. P-gp inhibitors that have been reported to also interact with BCRP are for example GF120918 (elacridar),[34] cyclosporin A,[35] reserpin[36] and tariquidar.[37,38] A dual specific inhibitor could be advantageous for reversing resistance to drugs that are substrates of both transporters.

In our laboratory, tariquidar (XR9576) served as a template to design new MDR modulators.[39,40] In recently published studies, we presented the pharmacological results of these compounds in relation to P-gp.[39,40] The biological activity data were obtained in the new Hoechst 33342 assay and the well established Calcein AM assay. 3D-QSAR models were generated by CoMFA and CoMSIA and yielded an internal predictive squared correlation coefficient higher than 0.8. The best models were based on electrostatic, steric, hydrogen bond acceptor, and hydrophobic fields. Considering that tariquidar inhibits not only P-gp function but also is a powerful BCRP modulator,[29] we decided to determine the inhibitory potencies of five XR-derivatives and 25 newly synthesized structurally related compounds towards BCRP function. In this study we present their inhibitory activities determined in BCRP overexpressing tumor cells. The inhibitory potencies of these substances were determined in the new Hoechst 33342 assay described previously[39] that was transferred to BCRP overexpressing cells. 3D-QSAR models using CoMFA and CoMSIA methodologies were generated and validated applying different techniques: the scrambling stability test, the leave-one-out, and leave-many-out cross-validation. The best models yielded internal predictive squared correlation coefficients of higher than 0.8. These models may serve as useful tools for the rational design of new BCRP inhibitors. To our knowledge this is the first 3D-QSAR study in relation to BCRP inhibitors. One additional, pivotal aim of this study was to compare the biological activity data of these compounds determined in P-gp overexpressing cells on one side and BCRP overexpressing cells on the other side. The intention of this comparison was to answer the question whether these substances inhibit P-gp and BCRP with identical potency, or not. The results may support a better insight which structural features direct an interaction with P-gp and/or BCRP.

2. Results

2.1. Functional assays

For a selective investigation of BCRP it was important to illustrate that the MCF-7 MX cell line overexpresses the ABCG2 gene product BCRP only. As shown in different studies by several working groups the mitoxantrone-resistant MCF-7 MX cell line is supposed to express high levels of BCRP.[41–44] In this study, the overexpression of BCRP was proven applying the specific anti-BCRP monoclonal BXP-21 antibody and fluorescein-conjugated anti-mouse antibody with flow cytometry detection.[45–47] In contrast to MCF-7 MX cells, the cell lines MCF-7, A2780, and A2780adr show no detectable levels of BCRP (Fig. 1). In MCF-7 MX cells no overexpression of the ABCB1 gene product P-gp was detected using a selective FITC-labeled P-gp antibody and flow cytometry.[48,49] Adriamycin resistant A2780adr cells served as a positive control containing high levels of P-gp as indicated by strong fluorescence intensity (Fig. 1). As the fluorescence intensities of MCF-7 MX, MCF-7, and A2780 cells were comparable to the background fluorescence intensity, the level of P-gp expression in these cell lines was negligible. These results agree with literature data.[41–44]

To determine BCRP activity, we transferred the newly developed Hoechst 33342 assay[39,40] to BCRP overexpressing MCF-7

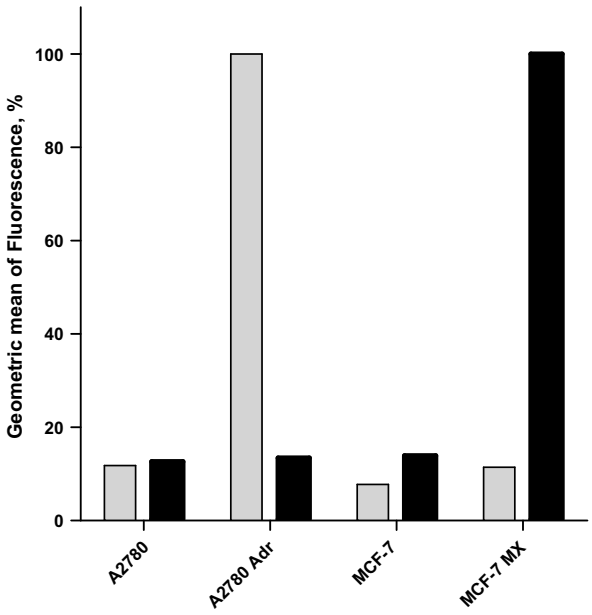

Figure 1. Proof of overexpression of P-gp (shown in gray) and BCRP (depicted in black) using the P-gp-specific antibody MRK-16 and the BCRP-specific antibody BXP-21 and a secondary fluorescein-conjugated anti-mouse antibody applying flow cytometry detection. Data indicate that P-gp is overexpressed in A2780adr cells, BCRP is overexpressed in MCF-7 MX cells. The other cell lines contain no significant levels of P-gp or BCRP.

MX cells. Two physicochemical properties of Hoechst 33342 enable the accomplishment of the assay in a simplified way: the strong tendency of Hoechst 33342 to penetrate into the cell membrane and the extreme milieu dependency of its fluorescence intensity. As shown in several studies, the fluorescence intensity of Hoechst 33342 increases enormously when localized in a lipophilic environment like the plasma membrane or bound to DNA.[50–53] Therefore the cellular fluorescence can be used as measure of Hoechst 33342 concentration in the membrane without the necessity of prior washing steps.[39,40]

To assess the influence of BCRP activity fluorescence–time curves were recorded using the BCRP overexpressing cells (MCF-7 MX) and the parental cell line MCF-7. Figure 2 shows different fluorescence–time curves of Hoechst 33342 obtained in MCF-7 and MCF-7 MX cells. The large difference of the two curves referring to MCF-7 (open circles) and MCF-7 MX cells (closed squares) without modulator is obvious. A total inhibition of BCRP function can be achieved by preincubating MCF-7 MX cells with 5.6 μM of compound **3** (XR9577).[54] The fluorescence–time curve obtained for MCF-7 MX cells in presence of XR9577 (closed circles) is comparable to that for MCF-7 cells. The strong difference of the fluorescence–time curves of MCF-7 MX cells without XR9577 and preincubated with XR9577 underlines that BCRP is highly active effluxing Hoechst 33342. This observation corresponds to several other studies, pointing out that Hoechst 33342 is also a BCRP substrate.[55–57] The fluorescence–time curve of MCF-7 cells in presence of 5.6 μM XR9577 is almost identical to the curve without modulator (open circles) confirming indirectly that the parental cell line does not express BCRP. Further, these results prove that the accumulation of Hoechst 33342 in the parental cell line is not influenced by compound **3** in an unspecific way by unspecific membrane effects.

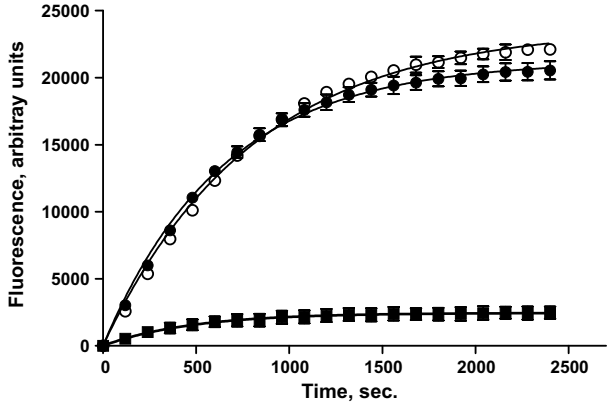

Figure 2. Fluorescence–time curves of Hoechst 33342 (final concentration 5 μM): MCF-7 MX cells without modulator (closed squares), MCF-7 MX cells, preincubated with 5.6 μM of compound **3** (XR9577) (closed circles) and MCF-7 cells without modulator (open circles). The fluorescence–time curve of MCF-7 cells preincubated with 5.6 μM of compound **3** (XR9577) overlaps the curve without modulator and is omitted for clarity.

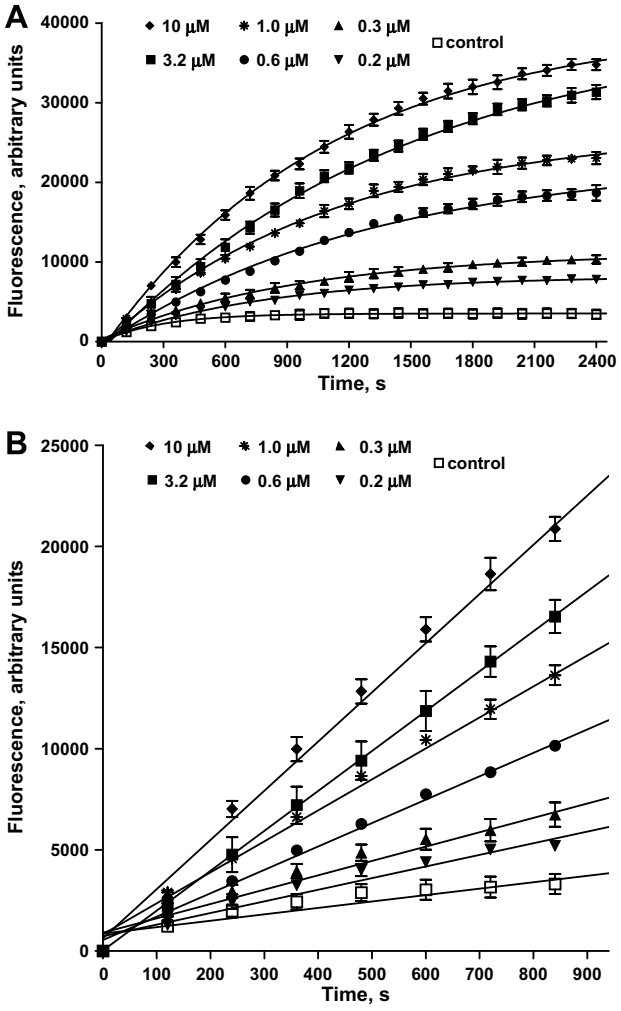

Figure 3. (A) Fluorescence–time curves for different concentrations of compound **3** (XR9577) determined with the Hoechst 33342 assay in MCF-7 MX cells. Fluorescence–time curves were analyzed based on one-phase exponential association analysis. Data illustrated are averages ± SE of a typical experiment with four replicates taken out from a series of four independent experiments. (B) Initial part of the fluorescence–time curves for different concentrations of compound **3** (XR9577) with the Hoechst 33342 assay in MCF-7 MX cells. Slopes were determined by linear regression. Presented data are averages ± SE from one typical experiment with four replicates belonging to a series of four independent experiments.

As shown in Figure 3A, typical fluorescence–time curves for several concentrations of compound **3** follow an exponential profile. Figure 3B contains the initial quasi-linear part of the different fluorescence–time curves from Figure 3A. Obviously, two different analyses are possible to perform: (i) the upper plateau values, Y_{max} values, of the fluorescence–time curves (when measuring fluorescence longer, compare Fig. 3A) can be determined and plotted versus the corresponding logarithmic concentrations (open squares, gray line). (ii) linear regression analysis (compare Fig. 3B) of the initial quasi-linear part (closed squares, black line). As to be expected and in accordance to a previous study[39] both analyses lead to no significant change in the pIC_{50} values: pIC_{50} (linear) = 6.08 ± 0.08, n_H = 1.49 ± 0.16; pIC_{50} (Y_{max}) = 6.17 ± 0.07, n_H = 1.62 ± 0.19, cf. Figure 4.

The inhibitory effect of the BCRP specific inhibitors novobiocin and Ko143 and seven known P-gp modulators was investigated in the established assay. The results are presented in Table 1. Comparing the BCRP inhibitory effects of these substances, the fumitremorgin C analogue Ko143 possesses the highest activity. Interestingly, the tyrosine kinase inhibitor imatinib is a rather potent BCRP inhibitor. It shows an approximately 10-fold stronger inhibition of BCRP function than novobiocin. All substances presented in Table 1 were also investigated in the Hoechst 33342 assay in relation to P-gp function using A2780adr cells. As expected, novobiocin and Ko143 did not lead to inhibition of P-gp function due to their assumed BCRP specifity. However, the known P-gp modulators were also weak inhibitors of BCRP function, with the exception of the tyrosine kinase inhibitor imatinib that proved to be an equipotent inhibitor of both transporters. Figure 5 shows a scatterplot of the pIC_{50} values for the seven substances active against both transport proteins determined with the Hoechst 33342 assay using BCRP and P-gp overexpressing cells. The correlation coefficient was calculated as 0.17, emphasizing no correlation between the inhibitory activities against both transporters (Fig. 5). These results may underline that the binding-sites of both ABC-transporters are different and various structural properties direct an interaction with P-gp and/or BCRP.

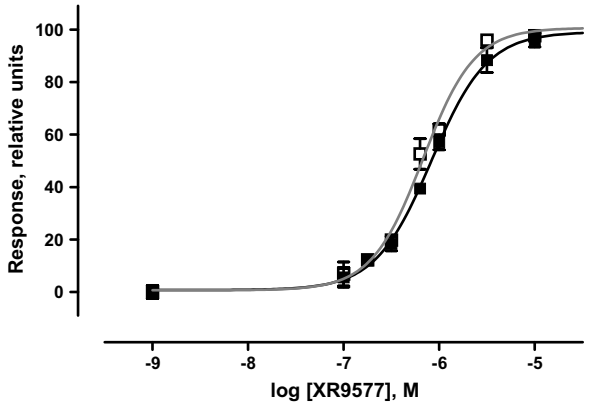

Figure 4. Comparison of concentration-response curves generated for compound **3** (XR9577) in MCF-7 MX cells obtained with the Hoechst 33342 assay by using (i) linear regression analysis of the initial quasi-linear part (closed squares, black line), (ii) the Y_{max} values derived from one-phase exponential association analysis (open squares, gray line): pIC_{50} (linear) = 6.08 ± 0.08, n_H = 1.49 ± 0.16; pIC_{50} (Y_{max}) = 6.17 ± 0.07, n_H = 1.62 ± 0.19. Data shown are averages ± SE from one typical experiment with four replicates out of a series of four independent experiments.

Table 1
pIC_{50} values of different substances in the Hoechst 33342 assay in relation to P-gp and BCRP function

Compound	pIC_{50} ± SD (P-gp)	pIC_{50} ± SD (BCRP)
Cyclosporine A	5.85 ± 0.09	4.20 ± 0.10
Diltiazem	4.37 ± 0.25	3.07 ± 0.08
Imatinib	5.14 ± 0.27	5.31 ± 0.18
Ko143	n.e.*	6.51 ± 0.15
Nicardipine	5.32 ± 0.13	4.78 ± 0.03
Novobiocin	n.e.	4.18 ± 0.15
Progesterone	4.32 ± 0.07	3.90 ± 0.24
Reserpine	5.49 ± 0.09	4.58 ± 0.13
Verapamil	5.34 ± 0.24	3.28 ± 0.06

Data shown are averages ± SD (n.e., no effect detectable up to 300 μM. n.e.*, no effect detectable up to 30 μM).

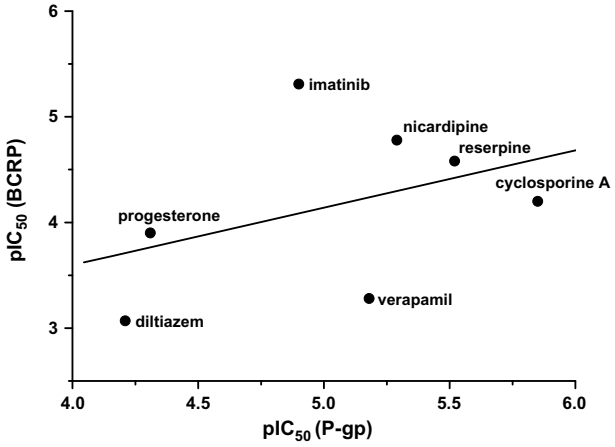

Figure 5. Scatterplot of the pIC_{50} values determined with the Hoechst 33342 assay in relation to BCRP (MCF-7 MX cells) and P-gp inhibition (A2780adr cells). Data shown are averages ± SD of at least three independent experiments. The squared correlation coefficient is 0.17.

Investigations of Robey et al. revealed that the 3rd generation modulator tariquidar (XR9576) is also capable to inhibit BCRP function.[37] This observation prompted us to investigate a series of structurally related substances synthesized in our laboratory, which had been identified as P-gp inhibitors,[40] also for their BCRP inhibitory potency. The studied series contained 25 newly synthesized derivatives and five XR analogues. Table 2 presents the structures and inhibitory potencies of these compounds towards BCRP function, and additionally includes the pIC_{50}-values against P-gp. The biological activity data towards P-gp were mostly presented and discussed in a previous study.[40] The whole dataset can be divided into two different classes according to the different template structures as shown in Table 2. Template 1 is common to the six anthranilamide derivatives compounds **1** to **6**. Template 2 depicts the basic structure of the remaining 24 compounds. All modulators possess a common tetrahydroisoquinoline-ethyl-phenyl-amide substructure. Comparison of the pIC_{50} values of the 30 compounds determined in P-gp overexpressing A2780adr cells and in BCRP overexpressing MCF-7 MX cells yields a moderate correlation (R^2 = 0.62) as visible in Figure 6. More than half of the compounds fall outside the 95 % confidence interval, underlining that different structural features direct an interaction with P-gp and/or BCRP.

2D- and 3D-QSAR analysis support to point out the main structural properties directing an interaction with P-gp or BCRP. Free-Wilson analyses[58] were performed to identify the structural elements influencing significantly the inhibitory effect against P-gp and BCRP function. Table 3 represents the structural features used as variables in the Free-Wilson analyses and lists the compounds containing the structural elements. After removal of compounds possessing singular variables, 15 could be included in the Free-Wilson analysis. The final models were derived applying the significant variables only. The results are presented in Table 4. They illustrate that methoxy groups in positions 6 and 7 of the tetrahydroisoquinolinylamide substructure contribute statistically significant to P-gp inhibition. However, a negative impact of the methoxy

Table 2
Structures and biological activity data of the investigated compounds

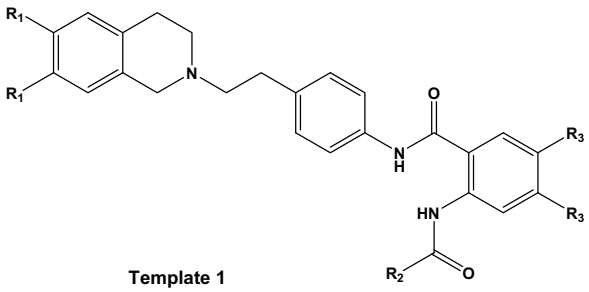

Template 1

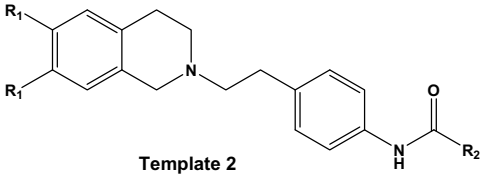

Template 2

Compound no.	R_1	R_2	R_3	pIC_{50} ± SD (BCRP)	pIC_{50} ± SD (P-gp)[a]
Template 1					
1 (XR9456)	OCH_3	Phenyl	H	5.40 ± 0.13	6.29 ± 0.06
2 (XR9544)	OCH_3	3-Quinolinyl	H	5.30 ± 0.19	6.78 ± 0.09
3 (XR9577)	H	3-Quinolinyl	H	6.00 ± 0.23	6.45 ± 0.07
4 (XR9504)	OCH_3	4-Methylphenyl	H	5.41 ± 0.25	6.28 ± 0.23
5 (XR9576)	OCH_3	3-Quinolinyl	OCH_3	5.84 ± 0.04	7.14 ± 0.12
6	OCH_3	3,4-Dimethoxyphenyl	H	5.68 ± 0.12	6.48 ± 0.15
Template 2					
7	OCH_3	2-Nitrophenyl	H	3.96 ± 0.15	5.26 ± 0.03
8	H	2-Nitrophenyl	H	4.10 ± 0.09	4.87 ± 0.02
9	OCH_3	2-Aminophenyl	H	4.07 ± 0.18	4.95 ± 0.24
10	H	2-Aminophenyl	H	4.13 ± 0.23	5.02 ± 0.04
11	OCH_3	4-Nitrophenyl	H	5.12 ± 0.18	5.86 ± 0.06
12	H	4-Nitrophenyl	H	5.18 ± 0.20	5.30 ± 0.16
13	OCH_3	4-Aminophenyl	H	3.58 ± 0.17	5.15 ± 0.09
14	H	4-Aminophenyl	H	4.11 ± 0.12	5.38 ± 0.32
15	OCH_3	3-Quinolinyl	H	4.62 ± 0.17	6.84 ± 0.25
16	H	3-Quinolinyl	H	5.30 ± 0.09	6.38 ± 0.09
17	OCH_3	3,4-Dimethoxyphenyl	H	4.32 ± 0.07	5.27 ± 0.25
18	OCH_3	4,5-Dimethoxy-2-nitro-phenyl	H	4.19 ± 0.05	5.31 ± 0.14
19	OCH_3	4-Quinolinyl	H	4.44 ± 0.15	5.65 ± 0.27
20	OCH_3	Benzo-1,3-dioxole	H	4.82 ± 0.14	5.85 ± 0.19
21	OCH_3	2-Bromophenyl	H	4.66 ± 0.05	5.46 ± 0.54
22	OCH_3	3-Bromophenyl	H	4.64 ± 0.21	5.49 ± 0.63
23	OCH_3	4-Bromophenyl	H	4.94 ± 0.02	5.61 ± 0.37
24	OCH_3	Phenyl	H	4.61 ± 0.09	5.32 ± 0.27
25	OCH_3	1-Naphthyl	H	4.89 ± 0.13	5.73 ± 0.18
26	OCH_3	2-Naphthyl	H	5.14 ± 0.10	6.11 ± 0.37
27	OCH_3	2-Quinoxalinyl	H	5.22 ± 0.20	6.68 ± 0.16
28	OCH_3	3-Isoquinolinyl	H	5.22 ± 0.10	6.11 ± 0.20
29	OCH_3	3-Pyridyl	H	4.35 ± 0.05	5.50 ± 0.23
30	OCH_3	6-Quinolinyl	H	4.84 ± 0.07	6.13 ± 0.21

[a] P-gp inhibition values are taken from Ref. 38 and are included for comparison, except those for compounds **5** and **24** that were determined in this study.

groups is observed in relation to BCRP indicated by the negative regression coefficient. Consequently, the elimination of methoxy groups in positions 6 and 7 of the tetrahydroisoquinoline substructure can strengthen the interaction with BCRP. Three substructures – the *para*-nitro-group, the change of a monocyclic substituent into a bicyclic substituent R_2 of template 1 (compare Table 2), the addition of a second amide linker – have a positive impact to the inhibitory potencies for P-gp and BCRP, respectively. Interestingly, the regression coefficients for the second amide linker are comparable, whereas the remaining regression coefficients for the 3-quinoline (R_2) and the para-nitro substituent (R_2) are different. The following conclusions are possible: (i) the introduction of an electrophilic substituent as the nitro group (-I- and -M-effect) increases in a more distinctive way the BCRP inhibitory potency than the P-gp inhibitory effect. (ii) The differences of the regression coefficients for the 3-quinoline substructure (R_2) illustrate that this structural element enhances a preferred interaction with P-gp. Further, including methoxy groups in positions 3 and 4 (R_2) reveals a weak increase of the pIC_{50} value in relation to BCRP, but not to P-gp.

Despite the fact that lipophilicity presents an important parameter related to incorporation into the membrane and to interaction with the drug binding site(s) of the proteins, no correlation was found between the inhibitory potencies and the calculated log *P* values (data not shown). Further, the calculated log*D* values and the pIC_{50} values show also no correlation (data not shown).

The span in activity data of two logarithmic units, together with the well-balanced, homogeneous distribution of the inhibitory potencies over the activity range represent some central pre-conditions to perform 3D-QSAR analyses including CoMFA and CoMSIA approaches. A crucial factor in 3D-QSAR analysis like CoMFA or CoMSIA is the alignment of the compounds. To facilitate comparison with our previous results, the same alignment as in Ref. 39 was chosen. Table 5 summarizes the results of the 3D-QSAR analyses based on LOO (leave-one-out) cross-validation.[59] All single fields and all possible field combinations were calculated. The calculations were accomplished both for P-gp and BCRP-related biological activity data. The results of the 3D-QSAR models served to get a better insight which structural properties are necessary for an efficient interaction with P-gp or BCRP or both transporters. The best models are marked in bold in Table 5. For both transporters the CoMSIA methodology yielded models with superior statistics as compared to CoMFA. For BCRP inhibition, the highest cross-

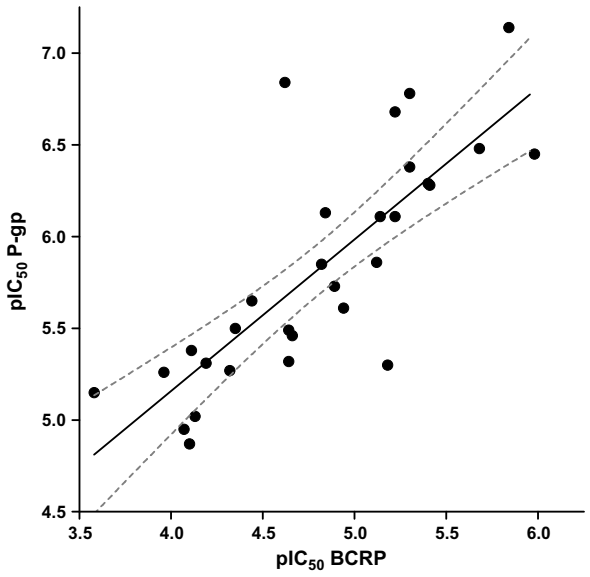

Figure 6. Scatterplot of the pIC_{50} values generated with the Hoechst 33342 assay on BCRP (MCF-7 MX cells) and P-gp (A2780adr cells). The explained variance is 0.62 for all 30 compounds. Data shown are averages ± SD of at least three independent experiments.

validated squared correlation coefficients q^2 were obtained for the combination of electrostatic and donor field ($q^2 = 0.801$, $n_{opt} = 4$). The additional inclusion of the steric field led to a further small increase in q^2 (sed-model: $q^2 = 0.803$, $n_{opt} = 4$). Models without the donor field were generally of lower statistical quality. For CoMFA derived models a similar pattern was obtained. The additional consideration of the H-bond field led to significantly better models. For P-gp inhibition, the best CoMSIA models were based on the following field combinations: electrostatic and acceptor ($q^2 = 0.866$, $n_{opt} = 4$) and electrostatic, acceptor, and steric ($q^2 = 0.863$, $n_{opt} = 4$). The addition of the hydrophobic field to these models led to a small, non-remarkable decrease of the corresponding q^2 values. The corresponding CoMFA models had again a lower internal predictivity, however, the difference was much less pronounced as for the BCRP inhibitory activity of the compounds. A slightly smaller but largely overlapping set of compounds has been analyzed previously for P-gp inhibitory potency by 3D-QSAR analysis.[40] It was therefore of interest to compare both analyses in order to estimate the influence of the newly introduced compound **24** and most active compound tariquidar on the outcome of the 3D-QSAR analysis. Comparison of the statistical indices obtained for the smaller subset analyzed in Ref. 39 with the values reported in Table 5 revealed that the ranking of the models remained unchanged, although the q^2 values are even higher now. The same fields led to the best models, emphasizing in this way the validity of the conclusions drawn from the previous analysis.

Figure 7A illustrates the plot of the predicted activity data from LOO cross-validation by the CoMSIA 'sed' model versus the measured activity data for BCRP inhibition. All compounds are predicted with similar precision and no extreme outliers are present. Figure 7B depicts the plot of the predicted inhibitory potencies based on the 'sea' model versus the observed inhibitory potencies against P-gp. The predictions are very satisfactory without outliers.

2.2. Contour plots

Contour plots were generated to visualize the contribution of the different fields to the biological activity of the studied compounds. Contour plots allow to gain more information from the models and to point out the differences between the BCRP and P-gp-related models. Figure 8 illustrates the contour plots of the most favorable model for steric, electrostatic, and donor fields for

Table 3
Free-Wilson matrix for 15 structurally related derivatives

Compound no.	pIC_{50} (P-gp)	pIC_{50} (BCRP)	R_1 6,7-dimethoxy	R_2 ortho-nitroph.	R_2 ortho-aminoph.	R_2 para-nitroph.	R_2 3,4-dimethoxyph.	R_2 3-quinoline	Amide linker 2
2 (XR9544)	6.78	5.30	1	0	0	0	0	0	1
3 (XR9577)	6.45	6.00	0	0	0	0	0	0	1
5 (XR9576)	7.14	5.84	1	0	0	0	1	0	1
7	5.26	3.96	1	1	0	0	0	0	0
8	4.87	4.10	0	1	0	0	0	0	0
9	4.95	4.07	1	0	1	0	0	0	0
10	5.02	4.13	0	0	1	0	0	0	0
11	5.86	5.12	1	0	0	1	0	0	0
12	5.30	5.18	0	0	0	1	0	0	0
13	5.15	3.58	1	0	0	0	0	0	0
14	5.38	4.11	0	0	0	0	0	0	0
15	6.84	4.62	1	0	0	0	0	1	0
16	6.38	5.30	0	0	0	0	0	1	0
17	5.27	4.32	1	0	0	0	1	0	0
18	5.31	4.19	1	1	0	0	1	0	0

Compound **14** (marked in gray) was defined as the reference substance for performing the multiple linear regression analysis (ph., phenyl; amide linker 2 refers to compounds containing template 1).

Table 4
Results of the Free-Wilson analyses of 15 compounds using significant variables only: statistical data, regression coefficients and their standard errors

	F value = 41.95, $R^2 = 0.959$, $R = 0.979$, SE of estimation = 0.19 Regression coefficient (BCRP)	F value = 45.21, $R^2 = 0.948$, $R = 0.973$, SE of estimation = 0.21 Regression coefficient (P-gp)
Constant	4.178 ± 0.092	4.969 ± 0.102
(R_1) 6,7-dimethoxy	−0.362 ± 0.109	+0.292 ± 0.111
(R_2) para-nitroph.	+1.153 ± 0.152	+0.465 ± 0.166
(R_2) 3,4-dimethoxyph.	+0.422 ± 0.139	–
(R_2) 3-quinoline	+0.963 ± 0.152	+1.495 ± 0.166
Amide-linker 2	+1.636 ± 0.128	+1.627 ± 0.143

Table 5
Statistical characteristics of the 3D-QSAR models using CoMFA and CoMSIA for BCRP and P-gp inhibition

Fields	BCRP					P-gp				
	LOO			NV		LOO			NV	
	q^2	SDEP	n	r^2	s	q^2	SDEP	n	r^2	s
CoMFA										
e	0.613	0.395	3	0.835	0.257	**0.833**	**0.277**	**5**	**0.962**	**0.132**
e h-bnd	0.732	0.339	4	0.934	0.166	0.685	0.389	6	0.963	0.133
h-bnd	0.707	0.350	4	0.920	0.183	0.542	0.433	2	0.779	0.301
s	0.525	0.432	3	0.743	0.321	0.757	0.325	3	0.892	0.215
s e	0.665	0.367	3	0.856	0.241	**0.823**	**0.290**	**4**	**0.951**	**0.147**
s e h-bnd	**0.757**	**0.321**	**4**	**0.949**	**0.147**	0.751	0.323	2	0.884	0.218
s h-bnd	**0.760**	**0.317**	**4**	**0.949**	**0.150**	0.720	0.338	2	0.875	0.226
CoMSIA										
a	0.549	0.436	3	0.702	0.346	0.570	0.436	4	0.764	0.323
d	0.558	0.424	3	0.649	0.376	0.439	0.498	4	0.551	0.446
d a	0.662	0.369	3	0.822	0.268	0.620	0.418	4	0.833	0.272
e	0.675	0.361	3	0.843	0.251	0.823	0.274	3	0.924	0.180
e a	0.599	0.402	3	0.773	0.302	**0.866**	**0.243**	**4**	**0.930**	**0.175**
e d	**0.801**	**0.283**	**4**	**0.917**	**0.187**	0.828	0.276	4	0.913	0.196
e h	0.698	0.368	5	0.902	0.206	0.815	0.293	5	0.948	0.154
e h a	0.635	0.398	3	0.814	0.274	**0.853**	**0.260**	**5**	**0.954**	**0.146**
e h d	0.783	0.296	3	0.878	0.221	0.822	0.292	6	0.945	0.163
e h d a	0.755	0.330	3	0.868	0.230	0.808	0.291	4	0.917	0.192
h	0.590	0.431	6	0.864	0.248	0.759	0.333	5	0.923	0.188
h a	0.609	0.483	5	0.865	0.242	0.761	0.332	5	0.916	0.196
h d	0.727	0.338	3	0.818	0.270	0.721	0.366	6	0.880	0.240
h d a	0.716	0.359	6	0.931	0.178	0.684	0.382	5	0.894	0.221
s	0.525	0.437	3	0.702	0.346	0.793	0.308	5	0.923	0.188
s a	0.544	0.428	3	0.725	0.333	0.802	0.296	4	0.872	0.238
s d	0.695	0.373	4	0.830	0.266	0.758	0.341	6	0.935	0.177
s e	0.684	0.356	3	0.837	0.256	0.842	0.275	5	0.955	0.144
s e a	0.602	0.400	3	0.772	0.302	**0.863**	**0.246**	**4**	**0.944**	**0.157**
s e d	**0.803**	**0.282**	**4**	**0.916**	**0.187**	0.824	0.279	4	0.917	0.192
s e h	0.678	0.374	5	0.895	0.213	0.826	0.285	4	0.899	0.241
s e h a	0.639	0.397	5	0.887	0.222	**0.857**	**0.251**	**4**	**0.918**	**0.190**
s e h d	**0.785**	**0.294**	**3**	**0.886**	**0.214**	0.806	0.296	3	0.896	0.210
s e h d a	0.749	0.320	3	0.874	0.225	0.813	0.282	3	0.909	0.197
s h	0.593	0.421	5	0.826	0.275	0.821	0.293	6	0.960	0.138
s h a	0.615	0.410	5	0.868	0.240	0.841	0.271	5	0.934	0.174
s h d	0.757	0.313	3	0.840	0.254	0.770	0.331	3	0.821	0.276

The best models are shown in bold.
Fields: s, steric; e, electrostatic; h-bnd, hydrogen bonds; h, hydrophobic; a, hydrogen bond acceptor; d, hydrogen bond donor fields.
Statistical parameters: q^2, cross-validated correlation coefficient; n, optimal number of components; SDEP, standard error of prediction; r^2, squared correlation coefficient; s, standard error of estimate.

inhibition of BCRP including the structures of compound **3** (A) and compound **15** (B). Green contoured areas mark the favorite influence of the steric field overlapping the 3-quinolinyl substituent of compound **3**. Among the 30 investigated substances, compound **3** is the most active representative containing the basic structure of template 1. A substructure falling together with the green favorable region of the steric field is typical for all the six compounds with an anthranilamide nucleus. Yellow areas of sterically disfavored regions are related to compounds possessing low biological activity. Three main yellow contours are visible (Fig. 8): two of them depicting the negative contribution of the methoxy groups in positons 6 and 7 of the tetrahydroisoquinoline substructure to the inhibitory potency. This structural element is for example present in compound **15** explaining its weak BCRP inhibitory activity. The blue contour of the electrostatic field indicates that a positive charge will increase activity, while negative charge in this position leads to a decrease of the pIC_{50} value. One blue region is located in the vicinity of the methoxy groups in positions 6 and 7 of the tetrahydroisoquinoline substructure. Close to substituents in *para*-position of the benzamide substructure, a red contour is visible indicating that negative charge will increase activity. This region may correspond to one of the oxygen atoms of a nitro substituent as present in the compounds **11** and **12**. This is in agreement with the finding that compounds with a para nitro group show higher pIC_{50} values than compounds with a para amino group. Further, the red contoured area could correspond to bicyclic substituents. It is possible to draw the conclusion that the red contour is originated from the electron rich sp^2 hybridized carbon atoms present in bicyclic substituents and describing their positive impact to inhibitory potency.

Among the 30 studied compounds, all six derivatives based on template 1 and only four derivatives containing template 2 (nos. **9**, **10**, **13**, and **14**) possess hydrogen bond donor functions additionally to the HB donor function of the amide group of the skeleton structure. Thus, the donor field visualized in magenta (favored) and orange (disfavored) colored regions is only related to the differences in biological activity data of these compounds. One can assume that the magenta region and the orange area indicate the positive contribution of this substructure to the inhibitory potency.

Figure 9 depicts the contour plots of the 'sea' model with the compounds **3** (A) and **15** (B) for steric, electrostatic, and acceptor fields enabling the best prediction of the P-gp related pIC_{50} values. In contrast to Figure 8, two green colored regions are visible pointing to the positive impact of steric bulk. Again, one of the two green areas refers to the substituent R_2 of the six anthranilamide derivatives containing template 1. Additionally, the second green region is due to compounds with template 2, which share a bicyclic ring system instead of a monocyclic one. In general, compounds with

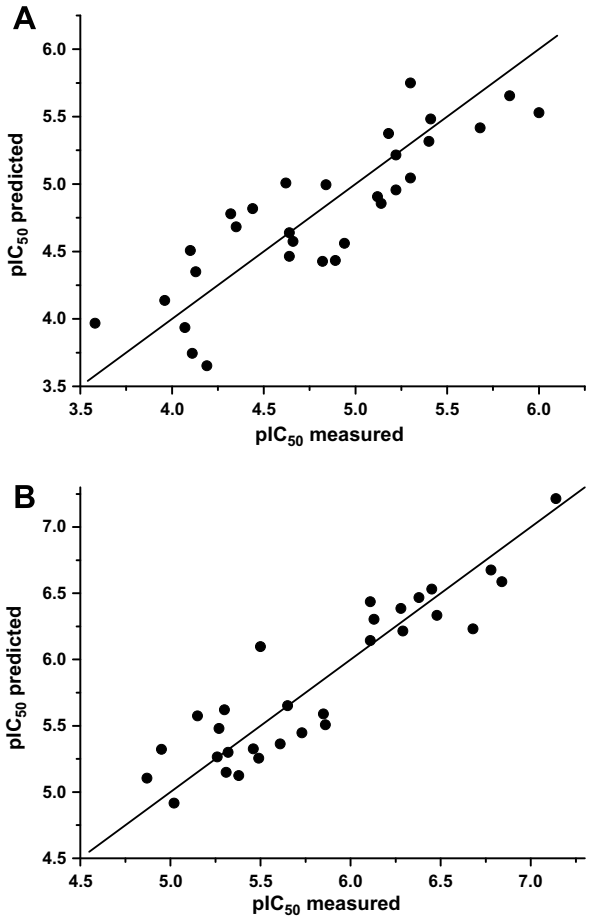

Figure 7. (A) Plot of observed versus predicted potencies for inhibition of BCRP. Predicted data were obtained with the 3D-QSAR model based on the 'sed' fields and applying LOO cross-validation. (B) Plot of the predicted pIC_{50} values against the measured pIC_{50} values for P-gp inhibition. The predicted inhibitory potencies were generated with the 3D-QSAR model based on the 'sea' fields and using LOO cross-validation.

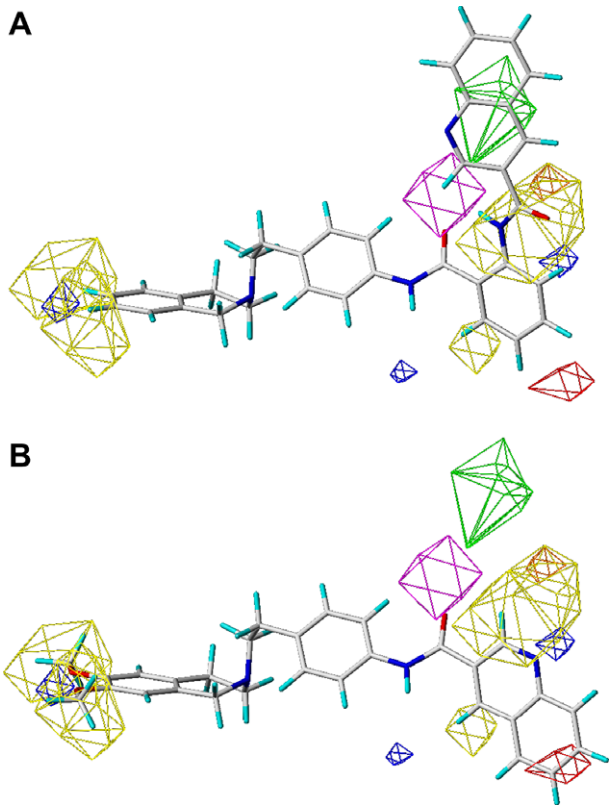

Figure 8. CoMSIA contour plot (STDEV*COEFF) of the 'sed' model (BCRP) with the most active compound **3** (A) and with compound **15** (B). Steric bulk is favored at green (85%) and disfavored at yellow (15%) regions. Positive charge is favored at blue (90%) and disfavored at red (15%). H-bond donor functionality is favored at magenta (80%) and disfavored at orange (20%).

a bicyclic substituent show a higher inhibitory potency than substances with monocyclic ring systems. The small red colored contour could reflect the favorable presence of negatively charged substituents (NO_2 group) as, for example, given in compounds **12** and **13**. But this red contour may correspond also to the impact of electron rich sp^2 hybridized carbon atoms of bicyclic substituents. All of the compounds containing template 2 and possessing bicyclic substituents show higher inhibitory potencies than corresponding substances with monocyclic substituents. Blue colored regions illustrate that negatively charged substituents in this position lead to a decrease of the biological activity. One blue colored area may correspond to hydrogen atoms of bicyclic substituents. These hydrogen atoms are all positively charged and this indicates in an indirect manner the positive influence of bicyclic substituents to the inhibitory potencies. Regions where hydrogen bond acceptor functions have a positive influence on the pIC_{50} value are colored in magenta. It is possible to draw the conclusion that the highly active compound **15** (as seen in Fig. 9 (B)) achieves its remarkable potency by a HB-acceptor interaction through its quinoline nitrogen. Unfavorable HB-acceptor interactions are expected in the orange contoured parts.

2.3. Validation of the best 3D-QSAR models

To further prove that the obtained models were not a result of chance correlation two different validation techniques were applied additionally to make a comparison with the previous results: the predictive power was also estimated by the leave-many-out method as internal validation using leave-one-out could lead to overoptimistic judgment of model quality. This problem can occur if compounds with comparable inhibitory potencies and (very) similar structural properties are present in the dataset. In such cases LOO-based models may fail when predicting real test molecules.[61] The leave-many-out technique is regarded as more robust and reliable than the leave-one-out procedure.[60,61] When performing LMO, the whole dataset is divided into several groups (5/4/3/2) of the same size. Under these conditions, only 80% down to 50% of the compounds are selected for model generation and then used to predict the inhibitory potencies of the remaining compounds. As the compounds are excluded from model generation randomly, the procedure has to be repeated several times (in this study 100 times) to get statistically valid results. The results for LMO cross-validation are summarized in Table 6. For the P-gp inhibition-related models, only a small decrease in q^2 is observed when going from LOO-validation to LMO with five groups. Even when the number of validation groups is decreased to three the q^2-values remain remarkably stable. Only at two groups a decrease in q^2-values is observed. For the models related to inhibition of BCRP initially a larger decrease in q^2 is found. This can be explained by the distribution of compounds with additional hydrogen bond donor properties. These are present in only 10 out of 30 compounds: all the six highly active compounds based on template 1, but only four compounds bearing template 2. This view is supported by the behavior of the q^2 values. The q^2 values only marginally drop by 0.03 when the number of cross-validation groups is decreased from five to three. Again only if 50% of the compounds are left

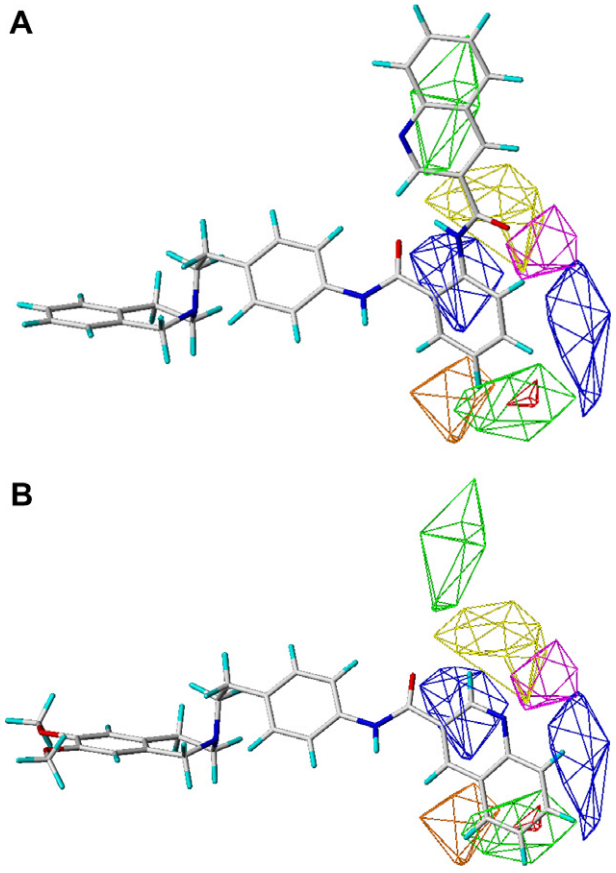

Figure 9. CoMSIA contour plot (STDEV*COEFF) of the 'sea' model referring to P-gp inhibition with the most active compound **3** (A) and with compound **15** (B). Favorable interactions: green 80% (steric), blue 90% (electrostatic), magenta 80% (donor). Non-favorable interactions: yellow 7% (steric), red 15% (electrostatic), orange 5% (donor).

Table 6
Validation of the best 3D-QSAR models: results of the leave-many-out validation method; averaged q^2 values and SD are based on 100 repetitions of the LMO procedure

Number of groups	CoMSIA fields			
	e d $q^2 \pm$ SD	e h d $q^2 \pm$ SD	s e d $q^2 \pm$ SD	s e h d $q^2 \pm$ SD
BCRP				
30 (LOO)	0.801	0.783	0.803	0.785
5	0.702 ± 0.138	0.684 ± 0.122	0.703 ± 0.139	0.694 ± 0.130
4	0.681 ± 0.145	0.631 ± 0.156	0.672 ± 0.156	0.634 ± 0.150
3	0.598 ± 0.181	0.586 ± 0.153	0.595 ± 0.144	0.570 ± 0.142
2	0.507 ± 0.228	0.420 ± 0.218	0.515 ± 0.194	0.469 ± 0.195
	e a $q^2 \pm$ SD	e h a $q^2 \pm$ SD	s e a $q^2 \pm$ SD	s e h a $q^2 \pm$ SD
P-gp				
30 (LOO)	0.866	0.853	0.863	0.857
5	0.841 ± 0.025	0.830 ± 0.029	0.842 ± 0.027	0.832 ± 0.033
4	0.828 ± 0.037	0.824 ± 0.033	0.833 ± 0.029	0.823 ± 0.040
3	0.813 ± 0.053	0.801 ± 0.052	0.808 ± 0.060	0.806 ± 0.065
2	0.759 ± 0.079	0.750 ± 0.087	0.736 ± 0.079	0.741 ± 0.074

To ease comparison the LOO values from Table 3 are additionally included.

out from model generation a noticeable drop in q^2 values is observed.

The scrambling stability test represents a second internal method to ensure the validity of 3D-QSAR models. To investigate the risk of chance correlations, the inhibitory potencies of the 30 compounds were randomly scrambled and the q^2 values calculated using LOO cross-validation. Again, the scrambling stability test has to be repeated several times to avoid chance results. According to the results presented in Table 7, no reliable predictions of the inhibitory potencies were possible based on scrambled activity data. Remarkably, all q^2 values in Table 7 are negative indicating that these models were without any predictive power.

3. Discussion

The Hoechst 33342 assay for the determination of P-gp activity, presented in a previous study,[39] was transferred in this study to the measurement of BCRP transport activity. The overexpression of BCRP in the cell line MCF-7 MX was confirmed in agreement with literature data.[41–44,54] Further, the absence of P-gp was proven in the used cell line. This is an essential precondition to assure a selective investigation of BCRP because Hoechst 33342 is also known to be a P-gp substrate.

To prove that the described Hoechst 33342 assay is an appropriate, simple test system to determine the inhibitory potencies of BCRP interacting compounds a set of twelve structurally unrelated substances was investigated using the BCRP-specific substrate Pheophorbide A by applying flow cytometry. Further, this approach enables us to find out whether the results obtained in the Hoechst 33342 assay were solely due to inhibition of BCRP function, or not. The strong correlation of the biological activity data illustrated in

Table 7
Validation of the best 3D-QSAR models: results of the scrambling stability test

Scrambling stability test	
CoMSIA fields	$q^2 \pm$ SD
BCRP	
e d	−0.208 ± 0.360
e h d	−0.218 ± 0.201
s e d	−0.201 ± 0.338
s e h d	−0.213 ± 0.204
P-gp	
e a	−0.218 ± 0.189
e h a	−0.205 ± 0.151
s e a	−0.222 ± 0.145
s e h a	−0.284 ± 0.249

Averaged q^2 values and SD refer to 100 randomly scrambled inhibitory potencies.

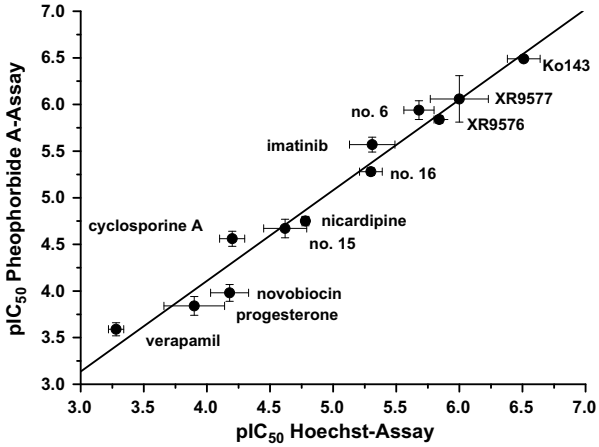

Figure 10. Comparison of inhibitory activities for twelve structurally unrelated compounds in the Pheophorbide A and Hoechst 33342 assays. The squared correlation coefficient is 0.97.

Figure 10 points out that the two different assays are suitable test systems to ascertain the inhibitory potencies of BCRP interacting compounds. Additionally, the strong correlation emphasizes that the results obtained were only due to a specific interaction with BCRP function. As the Hoechst 33342 assay is much simpler to perform, we used this assay for further investigations reported in this study.

A set of nine structural diverse compounds including Ko143 and novobiocin was investigated in the Hoechst 33342 assay for their ability to inhibit BCRP. To underline the validity of the Hoechst assay as an appropriate test system to determine the inhibitory potencies of potential BCRP modulators, the biological activity data of five BCRP interacting compounds were compared to the corresponding activity data taken from literature.[62] Matsson et al. yielded the fold increase values for different compounds using a mitoxantrone accumulation assay. The fold increase value was defined as the ratio of the mitoxantrone accumulation after coincubation with inhibitor to that observed in cells incubated with mitoxantrone alone. The obtained accumulation ratios were normalized to that ascertained with the potent and BCRP-specific modulator Ko143. One main disadvantage of this approach is the usage of only one concentration of the test compound (50 μM). Further, the calculated log fold increase values could only correlate with the pIC_{50} values determined in this study if the applied test concentration leads to an inhibition ranged between $\sim IC_{20}$ and IC_{80} (describing mostly the linear part of the sigmoidal concentration–response curve).[12] For the comparison of the inhibitory potencies, only log fold increase values higher than 0.47 were used. According to Matsson et al. this threshold value allows to differentiate between significant and non-significant BCRP modulation.[62] For five compounds fulfilling this requirement and overlapping with the present study, a strong correlation ($r^2 = 0.90$) of the biological activity data in the two test systems was found that is shown in Figure 11. Unfortunately, for the potent and specific BCRP modulator Ko143 only a fold increase value was reported by Matsson et al. applying 0.5 μM of Ko143. The use of a different test compound concentration prevents its inclusion into the correlation. Instead, the exact inhibitory potency for Ko143 ($IC_{50} = 0.19\ \mu M \pm 0.09$) was stated corresponding nicely to the IC_{50} value for Ko143 obtained in the Hoechst 33342 assay in this study ($IC_{50} = 0.31\ \mu M \pm 0.11/pIC_{50} = 6.51 \pm 0.15$). The agreement is quite impressive considering the factors that can influence the inhibitory activities determined as pIC_{50} values: (i) the IC_{50} value of a given inhibitor is dependent on the affinity of the substrate; (ii) the calculated IC_{50} values depend on the ratio of active transport to passive diffusion; (iii) however, the influence of the type of interaction between substrate and inhibitor (competitive or non-competitive) on IC_{50} values is expected to be small, as long as the used concentrations are below the substrate K_m.[63,39] Taking into account that the fold increase values were obtained in BCRP transfected cells and correlate well to the data yielded in the Hoechst assay in MCF-7 MX cells proves indirectly again that the biological activity data represent only an inhibition of BCRP function.

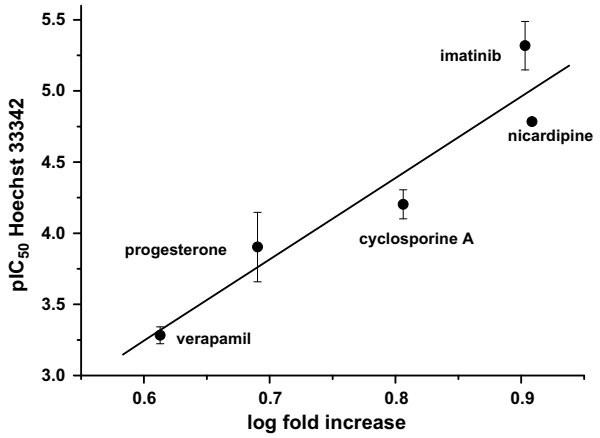

Figure 11. Scatterplot of the pIC_{50} values determined in the Hoechst 33342 assay and the log fold increase values taken from Ref. 62. The squared correlation coefficient is 0.90.

Among the studied standard compounds, not surprisingly, the fumitremorgin C analogue Ko143 was identified as the most potent BCRP modulator. Ko143 is known to interact with BCRP with high affinity, which has been proven in the past by different working groups.[31,65] The special, important role of Ko143 as a potentially clinical useful BCRP inhibitor is also due to its low in vivo toxicity (neurotoxicity) in contrast to fumitremorgin C. Regarding the biological activity data in relation to P-gp and BCRP (Table 1), two compounds were found to be BCRP-specific modulators, novobiocin and Ko143, in agreement with literature data.[31,64,23]

The tyrosine kinase inhibitor imatinib possesses a rather high inhibitory potency against BCRP. It has been previously shown by Ozvegy-Laczka et al. that only small concentrations of imatinib are necessary to inhibit BCRP function.[65] Additionally, imatinib showed a remarkable lower affinity to P-gp and MRP1. With regard on the high inhibitory potency of imatinib ascertained in the Hoechst 33342 assay, the outstanding position of this substance may be pointed out. Whether the substance achieves its high biological activity by interacting with the binding-site(s) in the transmembrane region or by an interaction with the ATP-binding site is still unclear and under debate.[65]

When comparing the pIC_{50} values of the structurally diverse substances towards P-gp and BCRP function, no correlation was found ($r^2 = 0.17$, Fig. 5) emphasizing that different structural properties are necessary for the interaction with P-gp and BCRP.

Recently it has been shown that the powerful P-gp modulator XR9576 is also capable to inhibit BCRP function.[57] In our laboratory XR9576 served as a lead structure to develop new, structurally related, and potent P-gp modulators.[54,66] The observation that tariquidar interacts with BCRP prompted us to study the inhibitory potencies of our derivatives also in relation to BCRP. Comparing the inhibition of P-gp and BCRP a squared correlation coefficient of $r^2 = 0.62$ was obtained, indicating a moderate correlation (Fig. 6). Again, it is illustrated that distinctive structural features play an essential role to strengthen an interaction with P-gp and/or BCRP.

To gain more detailed information how structural features influence the interaction with P-gp and/or BCRP 2D- and 3D-QSAR analyses were performed. The results of the Free-Wilson analyses underline the contrasting roles of the methoxy groups in positions 6 and 7 of the tetrahydroisoquinoline substructure. Further, the presence of *para*-nitrophenyl substituents in compounds based on template 2 (compounds **11** and **12**) force an interaction with BCRP. Interestingly, the introduction of the 3-quinoline substructure (compounds **15** and **16**) leads to a stronger interaction with P-gp. By comparing the regression coefficients for the amide linker 2, it is obvious that derivatives with template 1 show a more dual specific interaction with both transporters. However, for statistical reasons only 15 compounds were included into the Free-Wilson analyses. To prove whether these results hold true when including all thirty compounds 3D-QSAR analyses were carried out. To our knowledge, we present the first 3D-QSAR analysis of BCRP inhibitors. The best models were validated by the leave-many-out method and the scrambling stability test.[60,61] The main difference between the models for BCRP and P-gp inhibition is related to the contribution of the hydrogen bond properties. In the CoMSIA models for BCRP inhibition, the inclusion of the hydrogen bond donor field led always to an increase of the q^2 value. In contrast for

inhibition of P-gp, no positive contribution of the hydrogen bond donor field to the biological activity is found, and its inclusion is mostly associated with a decrease of the q^2 value. On the contrary, the inclusion of the hydrogen bond acceptor field is beneficial for P-gp inhibition. This indicates an important difference between the CoMSIA models referring to P-gp on one hand and to BCRP on the other hand. Hydrogen bond donor functions (not taking into account the amino group occurring in both templates 1 and 2) are only present in 10 compounds of the whole dataset: all anthranilamide derivatives and additionally the ortho–amino derivatives compounds **9** and **10** and further the para–amino analogues **13** and **14**. These four compounds containing template 2 show low BCRP inhibitory potencies which are not significantly different. As shown in Figure 8A, positive influence of the hydrogen bond donor field is not due to the para-amino substituted derivatives as a magenta colored region (donor field favored) is missing in this area. This underlines that the magenta marked contour can be explained by the positive impact of the amino group of the amide function given in anthranilamide derivatives. In general, these compounds have the highest pIC_{50} values among the investigated substances. With regard to the role of the hydrogen bond field to the P-gp-related 3D-QSAR models different suggestions are possible: compounds with the highest biological activities are found among template 1 and template 2 (compounds **15**, **16**, and **27**). Therefore, the impact of the amido group in anthranilamides to the inhibitory potency is supposed to be smaller. Considering the contour plots illustrated in Figure 9, the positive impact of the hydrogen bond acceptor field could be explained by the oxygen atom of the amide group in compounds of template 1 and/or by the 3-quinoline substituent in template 2-based structures (compounds **15** and **16**).

Most substances including methoxy groups in positions 6 and 7 of the tetrahydroisoquinoline substructure show smaller BCRP inhibitory potencies than their corresponding derivatives without methoxy groups. This observation is illustrated by the yellow marked region indicating the negative impact of the steric field to the biological activity. Further, the negative effect of the methoxy groups is again illustrated by a blue contoured region depicting the negative influence of negatively charged substituents. These results agree with the findings of the Free-Wilson analysis (Table 4). Interestingly, two potent P-gp modulators, compounds **15** and **27**, could be identified which possess low BCRP inhibitory potencies. These substances could be classified as modulators with preference for P-gp. Comparing the contour plots in Figures 8 and 9 it is obvious that the P-gp-related contour plot includes a second green colored region which indicates the positive effect of the steric field to an increase of the pIC_{50} value. This green area refers to compounds with template 2 which contain bicyclic substructures. Remarkably, this region is missing in the BCRP-related contour plot shown in Figure 8. A possible precondition to strengthen the interaction toward P-gp could be the introduction of a hydrogen bond acceptor group into the bicyclic ring structure as given in form of a nitrogen atom in the 3-quinoline substituent in template 2-based structures (compounds **15**, **16**, and **27**).

Figure 12 serves as a 'visualized' summary combining the results of the 2D- and 3D-QSAR analyses. It illustrates which structural elements direct an interaction with P-gp and/or BCRP. Blue 'plus-circles' describe the positive impact of structural features, which strengthen the P-gp inhibitory potencies of the investigated compounds. Orange colored circles show the influence of certain structural elements on the interaction with BCRP.

In conclusion, in this study the Hoechst 33342 assay which was applied to assess the potency of modulators and substrates interacting with P-gp was transferred to BCRP overexpressing cells to determine BCRP activity. The comparison of the biological activity data for nine different structurally unrelated compounds against P-gp and BCRP function pointed out that different structural properties lead to a better interaction with P-gp and/or BCRP. Results for a set of thirty structurally related derivatives which have been synthesized in our laboratory and pharmacologically characterized as P-gp and BCRP inhibitors revealed again, how distinct structural properties influence interaction with BCRP and/or P-gp. Our findings based on the results from 2D- and 3D-QSAR analyses can support the rational design of new and potent inhibitors.

4. Experimental

4.1. Chemicals

XR9576 (tariquidar) was a gift from Prof. Dr. Buschauer (University of Heidelberg, Germany). Ko143 was kindly provided by Dr. A. Schinkel (Amsterdam, The Netherlands). Doxorubicin was a gift from Medac (Hamburg, Germany), all other chemicals were purchased from Sigma Chemicals (Taufkirchen, Germany) unless otherwise stated.

The novel tetrahydroisoquinoline-ethyl-phenyl-amine-based MDR inhibitors, as well as the XR-derivatives, have been recently synthesized in our laboratory.[66] Stock solutions (10 mM) were prepared in DMSO.

4.2. Cell culture

The breast cancer resistant cell line MCF-7 MX and the parental cell line MCF-7 were kindly provided by Dr. E. Schneider, Wadsworth Center, Albany, NY, USA. Human ovarian carcinoma cell lines A2780 and the corresponding MDR1 overexpressing adriamycin

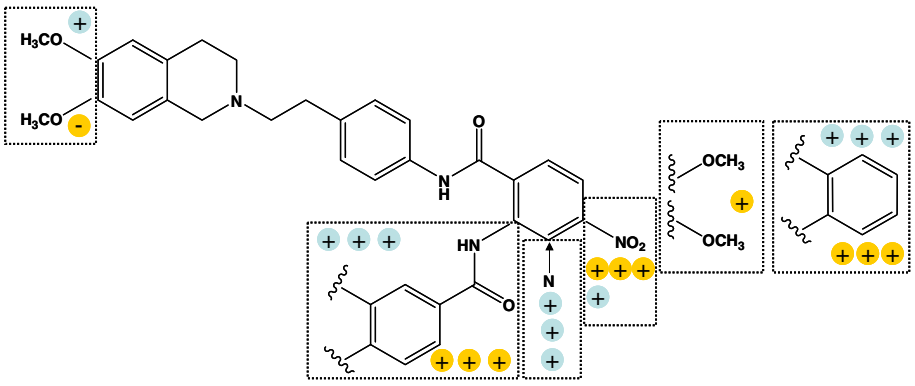

Figure 12. Summary of structural features of the investigated compounds that influence the interaction with BCRP and P-gp. Blue circles indicate the positive impact of structural elements to the P-gp inhibitory effect. Orange circles indicate the positive or negative effect on inhibition of BCRP.

resistant A2780adr cell line were purchased from ECACC (European collection of animal cell cultures, No. 93112519 [A2780], No. 93112520 [A2780adr], United Kingdom). The cell lines were grown in RPMI-1640 medium supplemented with 10% fetal bovine serum, 50 μl/ml streptomycin, 50 U/ml penicillin G, and 365 μl/ml L-glutamine.

Cells were incubated in a 5% CO_2 humidified atmosphere at 37 °C. When achieving a confluence of 80–90% cells were treated with trypsin–EDTA before subculturing. For MCF-7 MX cells every 5th passage mitoxanthrone (0.1 μM final concentration) was added to the cell culture medium to conserve ABCG2 overexpression. Before performing an experiment, mitoxanthrone was removed from the cell suspension and cells were cultivated at least one passage in the absence of the cytostatic drug. To A2780adr cells doxorubicin was added (0.1 μM final concentration) to maintain ABCB1 overexpression. The time interval and preprocessing procedure corresponded to the handling of MCF-7 MX cells, as described above.

4.3. Hoechst 33342 assay

Cell lines were cultivated under standard conditions in T75- or T175-flasks. After a confluence of 80–90% was reached, cells were harvested by gentle trypsination (0.05 % trypsin/0.02 % EDTA), then carried over into a 50 ml tube. After this step, cells were centrifugated (1200 rpm, 4 °C, 4 min). Subsequently, the cell pellet was resuspended in fresh culture medium, and the cell density was determined using a Casy I Modell TT cell counter device (Schaerfe System GmbH, Reutlingen, Germany). Followed by another centrifugation, cells were washed three times with Krebs–Hepes buffer and seeded into black 96-well plates (Greiner, Frickenhausen, Germany) at a density of approximately 20,000 cells per well in a volume of 90 μl when using MCF-7 MX cells. For the determination of the inhibitory potencies of substances interacting with P-gp A2780adr cells were seeded into black 96-well plates at a density of approximately 30,000 cells per well in a volume of 90 μl.

The plate was divided into two parts: the 1st, 3rd, 7th, and 10th column of the twelve columns of the 96-well plate (32 wells) only contained 90 μl Krebs–Hepes buffer, the remaining eight columns (64 wells) were filled up with 90 μl cell suspension. The 32 wells containing buffer were defined as 'background' wells. 10 μl of various test compounds in different concentrations were added to a total volume of 100 μl so that each concentration contained one 'background' well and two wells including cell suspension. The prepared 96-well plate was kept under 5% CO_2 and 37 °C for 30 min. After this preincubation period, 20 μl of a 30 μM Hoechst 33342 solution (protected from light) was added to each well.

Fluorescence was measured immediately in constant intervals (120 s) up to 2400 s at an excitation wavelength of 355 nm and an emission wavelength of 460 nm applying a 37 °C tempered BMG POLARstar microplate reader.

4.4. Assay data analyses

The fluorescence measured in the 'background' wells was subtracted from the fluorescence measured in the corresponding wells which were supplemented with cells. These data were applied for the following analysis: The slope of each fluorescence–time curve consisting of fluorescence-data points measured up to ~1000 s (initial part of the whole fluorescence–time curve) was calculated by linear regression and used as a dependent parameter. From these data, concentration–response curves were generated by non-linear regression using the four-parameter logistic equation with variable Hill slope (GraphPad Prism 5.0 software, San Diego, CA). For normalization of data, slopes from fluorescence–time curves were transformed to relative units by subtracting the lowest determined single value from all other data and thus setting it to zero. The highest measured single value was defined as 100% and all other data were normalized in that range.

4.5. Pheophorbide A assay

The MCF-7 MX cell line as well as its BCRP-negative counterpart MCF-7 (cell line) was cultivated and harvested according to the previously described Hoechst 33342 assay. To perform the Pheophorbide A assay, cells were counted and washed three times with Krebs–Hepes buffer. Eight hundred microliters containing 1 million cells were transferred into BD-FACS tubes. 100 μl of different test compound concentrations were added to cell suspension and incubated for 15 min in 37 °C tempered water bath. After the incubation period,Pheophorbide A was transferred into the tubes at a final concentration of 1 μM leading to a total volume of 1 ml. After this step, the fluorescence was measured immediately applying flow cytometry detection. The flow cytometer was equipped with an argon laser, Pheophorbide A was excited at an excitation wavelength of 488 nm, emission was detected in the FL_3 channel (633 nm). After measuring fluorescence, the different tubes were placed back into the water bath. The accumulation of Pheophorbide A was determined in 5 min intervals up to 60 min. At each time point the fluorescence was measured under the described conditions. The samples were measured until 10,000 events were counted or for 20 s. By gating on forward versus side scatter, debris and dead cells were eliminated. To assure specifity for BCRP, wild-type MCF-7 cells were also examined as a negative control.

The resulting fluorescence–time curves were analyzed using the one-phase exponential association model (GraphPad Prism 5.0 software, San Diego, CA). The Y_{max} values obtained by this approach were plotted against the corresponding logarithmic test compounds concentrations. Concentration-response curves were generated by non-linear regression using the four-parameter logistic equation. Data were normalized in accordance to the analysis of data obtained by the Hoechst 33342 assay.

4.6. Log*P* and log*D* calculations and Free-Wilson analyses

To calculate the log*P* and log*D* values of the compounds the program ACD[67] was applied. Multiple linear regression analysis was performed with SPSS version 14.0 for windows.[68]

4.7. CoMFA and CoMSIA specifications

To compare 3D-QSAR results in relation to P-gp and BCRP, the same alignment of the compounds as in our previous study was used.[40] In the CoMFA calculations, the following standard settings were used[59]: 2 Å regular grid size in all three directions within the automatically created grid box with 4 Å extension beyond the van der Waals volume of the overlaid molecules, an sp^3 carbon probe with +1 charge, and a distance dependent ($1/r$) dielectric constant. The following fields were calculated in CoMFA: steric (s), electrostatic (e), and hydrogen bond (h-bnd). The AM1 point charges were applied for calculation of the electrostatic fields. The standard energetic cutoff value of 30 kcal/mol with no electrostatic interactions at bad steric contacts was used. The threshold column filtering was set to 1.0 kcal/mol in all cases. In CoMSIA the following similarity indices fields were calculated: steric (s), electrostatic (e), hydrophobic (h), hydrogen bond donor (d), and hydrogen bond acceptor (a) with the default attenuation factor of 0.3 in the same grid box as used for CoMFA. A common probe atom with 1 Å radius and charge, hydrophobicity, and hydrogen bond property of +1 was used. The indices were evaluated according to the usual CoMSIA protocol with 1.0 column filtering. The CoMFA and CoMSIA QSAR equations were calculated by the partial least squares (PLS) method. The internal predictive power of the models was evaluated by

leave-one-out (LOO) cross-validation using the cross-validated correlation coefficient q^2, the optimal number of components n, and standard error of prediction SDEP. The linear regression fit was quantified by the squared correlation coefficient r^2 and the standard error of estimates.[59]

4.8. Validation of best 3D-QSAR models

Internal validation of the best 3D-QSAR models marked in bold in Table 5 was ensured by applying the leave-many-out procedure[60,61] (results shown in Table 6). The whole dataset was randomly divided into several groups (5/4/3/2), and the activity of the left-out compounds was predicted. This operation was repeated 100 times to exclude the possibility of chance correlations. The averaged squared cross-validated correlation coefficient and its standard deviation were calculated.

When performing the scrambling stability test,[60,61] the biological activity data were randomly scrambled (Table 7). To avoid chance correlations, the scrambling was repeated 100 times. After this step, the cross-validated correlation coefficient q^2 referring to the best fields highlighted in bold in Table 5 was calculated using leave-one-out cross-validation technique and averaged.

Acknowledgments

The authors thank Dr. A. H. Schinkel, The Netherlands Cancer Institute, Amsterdam, The Netherlands, for providing Ko143[32] and Dr. Armin Buschauer, Institute of Pharmaceutical Chemistry, University of Regensburg, Germany, for tariquidar. This work was supported by DFG (Deutsche Forschungsgemeinschaft) grants GRK677.

References and notes

1. Sarkadi, B.; Ozvegy-Laczka, C.; Nemet, K.; Varadi, A. *FEBS Lett.* **2004**, *567*, 116–120.
2. Fojo, T.; Bates, S. *Oncogene* **2003**, *22*, 7512–7523.
3. Bodo, A.; Bakos, E.; Szeri, F.; Varadi, A.; Sarkadi, B. *Toxicol. Lett.* **2003**, *140*, 133–143.
4. Borst, P.; Evers, R.; Kool, M.; Wijnholds, J. *J. Natl. Cancer Inst.* **2000**, *92*, 1295–1302.
5. Rao, V. V.; Dahlheimer, J. L.; Bardgett, M. E.; Snyder, A. Z.; Finch, R. A.; Sartorelli, A. C.; Piwnica-Worms, D. *Proc. Natl. Acad. Sci. U.S.A.* **1999**, *96*, 3900–3905.
6. Doyle, L. A.; Ross, D. D. *Oncogene* **2003**, *22*, 7340–7358.
7. Sarkadi, B.; Homolya, L.; Szakacs, G.; Varadi, A. *Physiol. Rev.* **2006**, *86*, 1179–1236.
8. Ling, R. L.; Juliano, V. *Biochim. Biophys. Acta* **1976**, *455*, 152–162.
9. Ling, V. P. *Am. J. Med.* **1995**, *99*, 31–34.
10. Schinkel, A. H.; Jonker, J. W. *Adv. Drug Deliv. Rev.* **2003**, *55*, 3–29.
11. Hoffmann, U.; Kroemer, H. K. *Drug Metab. Rev.* **2004**, *36*, 669–701.
12. Wiese, M.; Pajeva, I. K. *Curr. Med. Chem.* **2001**, *8*, 685–713.
13. Chen, C. J.; Chin, J. E.; Ueda, K.; Clark, D. P.; Pastan, I.; Gottesman, M. M.; Roninson, I. B. *Cell* **1986**, *47*, 381–389.
14. Ambudkar, S. V.; Dey, S.; Hrycyna, C. A.; Ramachandra, M.; Pastan, I.; Gottesman, M. M. *Annu. Rev. Pharmacol. Toxicol.* **1999**, *39*, 361–398.
15. Litman, T.; Brangi, M.; Hudson, E.; Fetsch, P.; Abati, A.; Ross, D. D.; Miyake, K.; Resau, J. H.; Bates, S. E. *J. Cell Sci.* **2000**, *113*, 2011–2021.
16. Kusuhara, H.; Sugiyama, Y. *Pflugers Arch.* **2007**, *453*, 735–744.
17. Doyle, L. A.; Yang, W. D.; Abruzzo, L. V.; Krogmann, T.; Gao, Y. M.; Rishi, A. K.; Ross, D. D. *Proc. Natl. Acad. Sci. U.S.A.* **1998**, *95*, 15665–15670.
18. Robey, R. W.; Polgar, O.; Deeken, J.; To, K. W.; Bates, S. E. *Cancer Metastasis Rev.* **2007**, *26*, 39–57.
19. Bailey-Dell, K. J.; Hassel, B.; Doyle, L. A.; Ross, D. D. *Biochim. Biophys. Acta* **2001**, *1520*, 234–241.
20. Diop, N. K.; Hrycyna, C. A. *Biochemistry* **2005**, *44*, 5420–5429.
21. Mohrmann, K.; van Eijndhoven, M. A. J.; Schinkel, A. H.; Schellens, J. H. M. *Cancer Chemother. Pharmacol.* **2005**, *56*, 344–350.
22. Takada, T.; Suzuki, H.; Sugiyama, Y. *Pharm. Res.* **2005**, *22*, 458–464.
23. Saito, H.; Hirano, H.; Nakagawa, H.; Fukami, T.; Oosumi, K.; Murakami, K.; Kimura, H.; Kouchi, T.; Konomi, M.; Tao, E.; Tsujikawa, N.; Tarui, S.; Nagakura, M.; Osumi, M.; Ishikawa, T. *J. Pharmacol. Exp. Ther.* **2006**, *317*, 1114–1124.
24. Staud, F.; Pavek, P. *Int. J. Biochem. Cell Biol.* **2005**, *37*, 720–725.
25. Chen, C. J.; Chin, J. E.; Ueda, K.; Clark, D. P.; Pastan, I.; Gottesman, M. M.; Roninson, I. B. *Cell* **1986**, *47*, 381–389.
26. Suzuki, M.; Suzuki, H.; Sugimoto, Y.; Sugiyama, Y. *J. Biol. Chem.* **2003**, *278*, 22644–22649.
27. Volk, E. L.; Schneider, E. *Cancer Res.* **2003**, *63*, 5538–5543.
28. Bates, S. E.; Robey, R.; Miyake, K.; Rao, K.; Ross, D. D.; Litman, T. *J. Bioenerg. Biomembr.* **2001**, *33*, 503–511.
29. Robey, R. W.; Medina-Perez, W. Y.; Nishiyama, K.; Lahusen, T.; Miyake, K.; Litman, T.; Senderowicz, A. M.; Ross, D. D.; Bates, S. E. *Clin. Cancer Res.* **2001**, *7*, 145–152.
30. Shiozawa, K.; Oka, M.; Soda, H.; Yoshikawa, M.; Ikegami, Y.; Tsurutani, J.; Nakatomi, K.; Nakamura, Y.; Doi, S.; Kitazaki, T.; Mizuta, Y.; Murase, K.; Yoshida, H.; Ross, D. D.; Kohno, S. *Int. J. Cancer* **2004**, *108*, 146–151.
31. Allen, J. D.; van Loevezijn, A.; Lakhai, J. M.; van der Valk, M.; van Tellingen, O.; Reid, G.; Schellens, J. H. M.; Koomen, G. J.; Schinkel, A. H. *Mol. Cancer Ther.* **2002**, *1*, 417–425.
32. Ahmed-Belkacem, A.; Pozza, A.; Muñoz-Martínez, F.; Bates, S. E.; Castanys, S.; Gamarro, F.; Di Pietro, A.; Pérez-Victoria, J. M. *Cancer Res.* **2005**, *65*, 4852–4860.
33. Imai, Y.; Tsukahara, S.; Asada, S.; Sugimoto, Y. *Cancer Res.* **2004**, *64*, 4346–4352.
34. Maliepaard, M.; van Gastelen, M. A.; Tohgo, A.; Hausheer, F. H.; van Waardenburg, R. C. A. M.; de Jong, L. A.; Pluim, D.; Beijnen, J. H.; Schellens, J. H. M. *Clin. Cancer Res.* **2001**, *7*, 935–941.
35. Qadir, M.; O'Loughlin, K. L.; Fricke, S. M.; Williamson, N. A.; Greco, W. R.; Minderman, H.; Baer, M. R. *Clin. Cancer Res.* **2005**, *11*, 2320–2326.
36. Zhou, S.; Schuetz, J. D.; Bunting, K. D.; Colapietro, A. M.; Sampath, J.; Morris, J. J.; Lagutina, I.; Grosveld, G. C.; Osawa, M.; Nakauchi, H.; Sorrentino, B. P. *Nat. Med.* **2001**, *7*, 1028–1034.
37. Robey, R. W.; Steadman, K.; Polgar, O.; Morisaki, K.; Blayney, M.; Mistry, P.; Bates, S. E. *Cancer Res.* **2004**, *64*, 1242–1246.
38. Mistry, P.; Stewart, A. J.; Dangerfield, W.; Okiji, S.; Liddle, C.; Bootle, D.; Plumb, J. A.; Templeton, D.; Charlton, P. *Cancer Res.* **2001**, *61*, 749–758.
39. Müller, H.; Klinkhammer, W.; Globisch, C.; Kassack, M. U.; Pajeva, I. K.; Wiese, M. *Bioorg. Med. Chem* **2007**, *15*, 7470–7479.
40. Müller, H.; Pajeva, I. K.; Globisch, C.; Wiese, M. *Bioorg. Med. Chem.* **2008**, *16*, 2448–2462.
41. van Hattum, A. H.; Schluper, H. M. M.; Hausheer, F. H.; Pinedo, H. M.; Boven, E. *Int. J. Cancer* **2002**, *100*, 22–29.
42. van Hattum, A. H.; Hoogsteen, I. J.; Schluper, H. M. M.; Maliepaard, M.; Scheffer, G. L.; Scheper, R. J.; Kohlhagen, G.; Pommier, Y.; Pinedo, H. M.; Boven, E. *Br. J. Cancer* **2002**, *87*, 665–672.
43. Volk, E. L.; Farley, K. M.; Wu, Y.; Li, F.; Robey, R. W.; Schneider, E. *Cancer Res.* **2002**, *62*, 5035–5040.
44. Volk, E. L.; Rohde, K.; Rhee, M.; McGuire, J. J.; Doyle, L. A.; Ross, D. D.; Schneider, E. *Cancer Res.* **2000**, *60*, 3514–3521.
45. Minderman, H.; Suvannasankha, A.; O'Loughlin, K. L.; Scheffer, G. L.; Scheper, R. J.; Robey, R. W.; Baer, M. R. *Cytometry* **2002**, *48*, 59–65.
46. Raaijmakers, M. H. G. P.; de Grouw, E. P. L. M.; Heuver, L. H. H.; van der Reijden, B. A.; Jansen, J. H.; Scheper, R. J.; Scheffer, G. L.; de Witte, T. J. M.; Raymakers, R. A. P. *Clin. Cancer Res.* **2005**, *11*, 2436–2444.
47. Maliepaard, M.; Scheffer, G. L.; Faneyte, I. F.; van Gastelen, M. A.; Pijnenborg, A. C. L. M.; Schinkel, A. H.; van de Vijver, M. J.; Scheper, R. J.; Schellens, J. H. M. *Cancer Res.* **2001**, *61*, 3458–3464.
48. Okochi, E.; Iwahashi, T.; Tsuruo, T. *Leukemia* **1997**, *11*, 1119–1123.
49. Aihara, M.; Aihara, Y.; Schmidtwolf, G.; Schmidtwolf, I.; Sikic, B. I.; Blume, K. G.; Chao, N. J. *Blood* **1991**, *77*, 2079–2084.
50. Tawar, U.; Jain, A. K.; Dwarakanath, B. S.; Chandra, R.; Singh, Y.; Chaudhury, N. K.; Khaitan, D.; Tandon, V. *J. Med. Chem.* **2003**, *46*, 3785–3792.
51. Tawar, U.; Jain, A. K.; Chandra, R.; Singh, Y.; Dwarakanath, B. S.; Chaudhury, N. K.; Good, L.; Tandon, V. *Biochem.* **2003**, *42*, 13339–13346.
52. Shapiro, A. B.; Ling, V. *J. Biol. Chem.* **1995**, *270*, 16167–16175.
53. Shapiro, A. B.; Ling, V. *J. Bioenerg. Biomembr.* **1995**, *27*, 7–13.
54. Jekerle, V.; Klinkhammer, W.; Scollard, D. A.; Breitbach, K.; Reilly, R. M.; Piquette-Miller, M.; Wiese, M. *Int. J. Cancer* **2006**, *119*, 414–422.
55. Ifergan, I.; Shafran, A.; Jansen, G.; Hooijberg, J. H.; Scheffer, G. L.; Assaraf, Y. G. *J. Biol. Chem.* **2004**, *279*, 25527–25534.
56. Doyle, L. A.; Ross, D. D. *Oncogene* **2003**, *22*, 7340–7358.
57. Clark, R.; Kerr, I. D.; Callaghan, R. Br. *J. Pharmacol.* **2006**, *149*, 506–515.
58. Free, S. M.; Wilson, J. W. *J. Med. Chem.* **1964**, *7*, 395–399.
59. SYBYL 6.9–7.3 versions; Tripos Inc., 1699 South Hanley Road, St. Louis, MO 63114-2917.
60. Tropsha, A.; Gramatica, P.; Gombar, V. K. *QSAR Comb. Sci.* **2003**, *22*, 69–77.
61. Höltje, H.-D.; Sippl, W.; Rognan, D.; Folkers, G. *Molecular Modeling*; Wiley–VCH: Weinheim, 2008.
62. Matsson, P.; Englund, G.; Ahlin, G.; Bergstrom, C. A. S.; Norinder, U.; Artursson, P. *J. Pharmacol. Exp. Ther.* **2007**, *323*, 19–30.
63. Segel, I. H. *Enzyme Kinetics*; Wiley: New York, 1976.
64. Su, Y.; Hu, P.; Lee, S.-H.; Sinko, P. J. *J. Pharm. Sci.* **2007**, *10*, 519–536.
65. Ozvegy-Laczka, C.; Hegedus, T.; Varady, G.; Ujhelly, O.; Schuetz, J. D.; Varadi, A.; Keri, G.; Orfi, L.; Nemet, K.; Sarkadi, B. *Mol. Pharmacol.* **2004**, *65*, 1485–1495.
66. Klinkhammer, W.; Design, Synthese und 3D-QSAR neuartiger P-gp-Modulatoren, Ph.D. Thesis, University of Bonn, 2006; http://deposit.ddb.de/cgi-bin/dokserv?idn=981124488&dok_var=d1&dok_ext=pdf&filename=981124488.pdf.
67. ACD/Labs, version 5.09, ACD pKa DB, Advanced Chemistry Development, Inc., Toronto, ON, Canada..
68. SPSS, version 14, SPSS, Chicago, IL, USA..